Available online at www.sciencedirect.com
SCIENCE DIRECT®
Nuclear Physics B (Proc. Suppl.) 132 (2004) 31–40
NUCLEAR PHYSICS B PROCEEDINGS SUPPLEMENTS
www.elsevierphysics.com

Theory of non-thermal phenomena in thin plasma sources: galaxy clusters, galaxies and supernova remnants

A.M. Bykov[a]

[a] A.F. Ioffe Institute for Physics and Technology, 194021, St. Petersburg, Russia

We review current models of energetic particle acceleration and nonthermal emission from objects of very different scales from clusters of galaxies through massive galaxies to supernova remnants. The nonthermal phenomena in clusters and massive galaxies are considered in the context of the hierarchical model of cosmic structure formation by accretion and merging of the dark matter (DM) substructures. The hierarchical model predicts interaction of sub-galactic scale DM halos with massive galaxies. The accretion and merging processes are producing gas shocks. Being the main gas-heating agent, large-scale shocks in the course of cluster/galaxy structure aggregation, could accelerate energetic particles by the same collisionless plasma relaxation processes. Nonthermal emission of the energetic particles in clusters and massive galaxies could be a test to constrain the DM minihalos properties. We also discuss X-ray emission from supernova remnants in a dense galactic environment with applications to deep observations of the Galactic Center region.

1. INTRODUCTION

Nonthermal emission is a generic feature of violent relaxation processes in systems with a powerful kinetic energy release. Being different in nature, physical processes of the powerful kinetic energy release in clusters of galaxies, AGNs, and supernova remnants (SNRs) are typically accompanied with collisionless shock waves of different scales. Energetic particle acceleration in the collisionless shocks is an efficient process transferring kinetic energy of the magnetohydrodynamic (MHD) shock flow into nonthermal particles. Recent multi-wavelength observations open a wide window to study clusters of galaxies, AGNs, massive galaxies and SNRs. The reported detections of hard nonthermal emission from clusters with *BeppoSAX* (e.g. [22]) stimulated the study of nonthermal processes in clusters. We discuss here some current models and observational results relevant to X/γ-ray emission and nonthermal phenomena in the objects with an accent on the role of fast moving substructure elements interacting with the ambient matter.

2. NONTHERMAL EMISSION FROM CLUSTERS OF GALAXIES

Cluster of galaxies are the most massive virialized systems known. The total mass of a cluster, M, can be as high as a few $10^{15}\,\mathrm{M}_\odot$. A megaparsec-scale system of that mass has the gravitational binding energy, $E \sim GM^2/R$, of the order of 10^{64} erg. That huge energy can be released in a cluster aggregation process with an average power $L_{\rm kin} \lesssim 10^{46}$ erg·s^{-1}. Clusters provide a powerful tool for studying the hierarchical structure, the mass density, and the chemical evolution of the Universe. In particular, they provide a good estimate of the dynamical mass density parameter (Ω_d) on a Mpc scale and the measure of the baryon density fraction in the Universe. They are also excellent tracers of the large-scale structure of the Universe.

Clusters of galaxies are very bright in keV-regime X-rays, with luminosities $L_{\rm T} \lesssim 10^{45}$ erg s^{-1} in the range 2–10 keV. The emission mechanism is *thermal bremsstrahlung*. For instance, the Coma cluster ($M \sim 2\times10^{15}\,\mathrm{M}_\odot$, $z = 0.0238$) has $L_{\rm T} \sim 5 \times 10^{44}$ erg s^{-1} and the average intercluster gas temperature $T \approx 8.2$ keV which roughly corresponds to the virial gas

doi:10.1016/j.nuclphysbps.2004.04.004

temperature. The thermal structure of clusters is inhomogeneous and some large scale structures (e.g. due to merging or accretion) are present.

The following facts provide clear evidence for nonthermal phenomena in clusters of galaxies:

(i) Some of the clusters have large faint diffuse radio-halos. The halos are seen in the range from 30 MHz to 4 GHz and have radio luminosities $L_{\rm R} \lesssim 10^{41}$ erg s^{-1} (e.g., [23,24]).

(ii) Five clusters (Coma, Virgo, A2199, A1795, A4059) show some excess of the extreme ultraviolet emission over the thermal hot gas component up to large radii. Recent EUV-image reconstruction of the *EUVE* and *ROSAT* data for these clusters support that conclusion [14] while some controversies still remain. The magnitude of the EUV-emission below 0.4 keV for the Coma cluster, is $L_{\rm EUV} \sim (1\text{–}2) \cdot 10^{43}$ erg s^{-1} [31]. The constraints on the containment of a warm 10^6 K gas, that were imposed by *XMM-Newton* observations of the clusters Sersic 159-03 [26], A1835 [43] and A1795 [53], make the thermal origin of the EUV-excesses somewhat problematic. On the other hand a substantial warm gas thermal emission was found in Coma [17]

(iii) The hard X-ray emission above 20 keV in excess of that produced by the thermal gas was reported from the Coma cluster with *BeppoSAX* [19]. The estimated $L_{\rm XNT}$ was $\sim 3 \times 10^{43}$ erg s^{-1}. A similar nonthermal excess was also reported for A2256 [20]. Study of the hard X-ray emission of A3667 with *BeppoSAX PDS* indicated only marginal evidence ($\sim 2.6\,\sigma$) for a nonthermal excess with an extrapolated upper limit for the 20–80 keV flux with a factor ~ 3.4 less than the nonthermal flux reported for Coma [21]. One should note, however, the higher redshift of A3667 ($z = 0.055$). *BeppoSAX MECS* data analysis by [25] revealed $\sim 3.3\,\sigma$ excessive emission (in the 8-10 keV range) over the best fit thermal model outside the central 0.3–0.4 Mpc of the cluster A2199 ($z = 0.0299$). The data were reanalyzed in [22] where only a marginal $\sim 2\,\sigma$ excess was found. A2199 is a regular shape cluster without any indications of recent merging activity. A reliable detection or significant constraint of the hard tails with *INTEGRAL* or *ASTRO-E2* would be very important to identify the nature of the nonthermal processes in clusters.

Gamma-ray emission has not yet been detected from clusters of galaxies. There are upper limits for the Coma cluster, imposed by *GRO OSSE* [47] and by *GRO EGRET* [51,45] of $L_\gamma < 10^{43}$ erg s^{-1} above 100 MeV.

2.1. Energetics of Nonthermal Processes

Assuming that the nonthermal emission described above is truly diffuse and of a quasi-steady nature rather than of a transient type, some general constraints can be imposed on possible models. It is expected that a substantial fraction of the kinetic energy release during the cluster aggregation should be emitted away as thermal X-ray emission. Thorough studies of the thermal emission in the 1–10 keV regime showed that the observed emission is consistent with that produced by a locally thermal thin plasma of a typical temperature below 10 keV, while some inhomogeneities are also present. The luminosity of the nonthermal emission above 20 keV discovered with *BeppoSAX* [19] in the Coma cluster is $\sim$ 5% of the thermal. The assumption that the emission above 20 keV is produced by nonthermal bremsstrahlung of non-relativistic electrons would imply a huge Coulomb loss power ($\sim 10^5 \times L_{\rm XNT}$) released into the intercluster medium [44]. That power is much higher than the average kinetic power $L_{\rm kin}$ and could only occur for a short period of time. A possible alternative scenario is the inverse Compton X-ray emission of relativistic electrons [46]. The presence of relativistic electrons in the clusters is proven by the detection of diffuse radio emission that is most likely due to synchrotron radiation (e.g. [24]). Here we shall consider some possible mechanisms of the kinetic power conversion to nonthermal particles during the cluster aggregation process. It is possible, however, that powerful activity of some AGNs or active starburst galaxies (during a relatively short time scale) could also contribute to a long-lived diffuse population of relativistic particles (at 10 – 100 MeV energies).

2.2. The Hierarchical Structure Model and Nonthermal Emission of Clusters

Growth of the hierarchical structure of the Universe as a result of merging and accretion of dark matter substructures is a generic feature of the cold dark matter (CDM) cosmogony (e.g. [61]). The cluster gas heating during the aggregation process in the hierarchical model is mainly due to large scale shocks produced by the fast motions of the cluster building blocks. The blocks are subclusters, galactic groups or individual galaxies. Optical observations (e.g. [60]) have revealed supersonic motions of some isolated galaxies in the relaxed clusters. High resolution radio and X-ray observations were used to study the merging phenomena in clusters. The NGC 4839 group falling into the Coma cluster was observed by *XMM-Newton* [39]. Evidence was found for a bow shock of scale $\lesssim$ 100 kpc and ram pressure stripping. A recent *Chandra* observation [55] revealed a moving "cold front" near the core of cluster A3667. The sharp discontinuity in the X-ray surface brightness of 500 kpc scale was considered as a boundary of a cold dense cloud of a near-sonic velocity with a possible weak bow shock at ~ 350 kpc ahead of the cold front. The model [49] of a peculiar large scale structure of A3667 considers a recent (~ 1 Gyr) merger event of the cluster with an 80% less massive subcluster. Multiple large scale shock generation accompanies the event.

Nonthermal particles in the clusters could originate from different kinds of sources including: (i) ejection by AGNs, radio or starburst galaxies, (ii) inelastic collisions of relativistic CR hadrons and (iii) particle acceleration/re-acceleration by large-scale shocks and turbulence. There is an extensive literature on the subject (see e.g. [3,13, 50,56,44,15,30,18] and references therein). Here we shall discuss a class of of nonthermal emission models considering conversion of kinetic energy released in the cluster assembling process.

Collisions of massive DM substructures during cluster aggregation would drive collisionless shocks in the gas component if the relative gas flow velocities are supersonic and superalfvenic. Large-scale shocks resulted from accretion onto filaments, sheets and knots in a matter distribution were simulated in [35] for both a standard CDM and a CDM model with cosmological constant. Strong cosmic shocks of sonic Mach numbers up to 10^3 were found to be formed during accretion onto filaments. Merging of substructures within galactic clusters produces flow shocks of lower (< 10) Mach numbers.

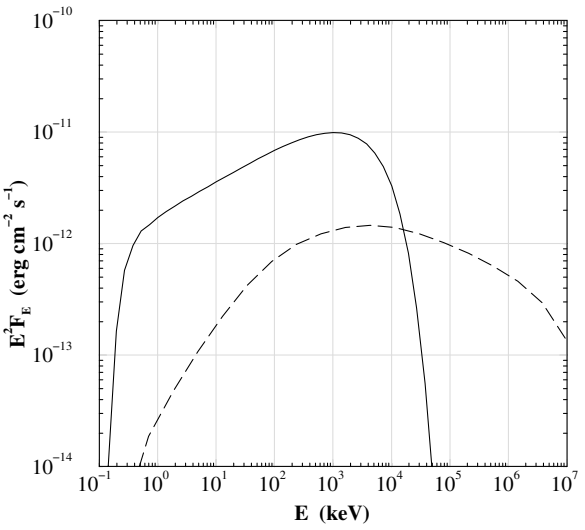

Figure 1. A modelled hard nonthermal emission spectrum of a cluster, after weighting individual halo spectra [9]. The model parameters are typical for the Coma cluster. The solid line denotes the inverse Compton emission from the CMB photons while the dashed line is the nonthermal bremsstrahlung.

Copious fast moving DM halos in virializing clusters could provide a plausible source for the extended nonthermal X-ray and γ-ray emission [9]. This follows from the fact that accelerated particles are produced in their bow shocks. A substantial fraction of a virialized ensemble of halos can have moderate supersonic velocities outside the central region of a rich cluster [41].

Dark matter halos of supersonic and superalfvenic velocities will create collisionless bow shocks of moderate Mach numbers $M \lesssim 3$, due to electromagnetic interaction between comoving baryonic matter and the hot intra-cluster

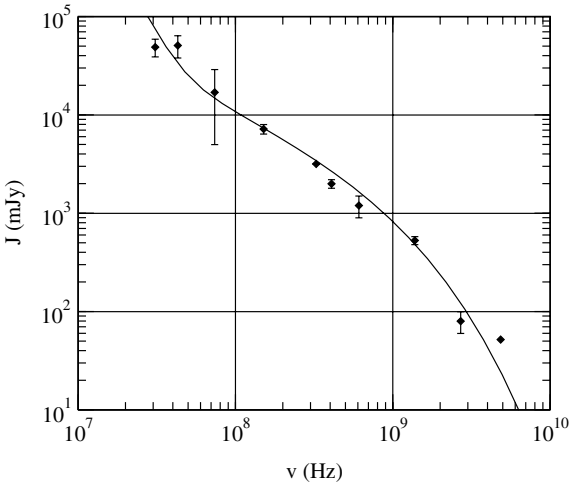

Figure 2. The modelled radio spectrum of a cluster, after weighting individual halo spectra [9]. The bow-shock Mach number distribution for the cluster was simulated in [41]. The model parameters are typical for the Coma cluster, of which flux measurements are shown [23].

gas. The amount of comoving baryonic matter depends upon the balance between ram-pressure stripping and replenishment rates. Particles are accelerated/re-accelerated locally by passing shocks, producing the observed nonthermal emission with a rather high efficiency. To simulate the spectra of nonthermal electrons in the galactic halo a kinetic equation was solved for the distribution function of the electrons, accounting for injection, diffusive transport, advection, the first and the second order Fermi acceleration and synchrotron and Coulomb losses [9].

There are three zones in the model: the preshock region, the shock transition region, and the post-shock flow, from where nonthermal emission from shock-accelerated particles originates. The particle distribution is inhomogeneous in the post-shock flow. The energy spectrum of the nonthermal electrons in the galactic halo is shaped by the joint action of the first and second order Fermi acceleration in a turbulent plasma with substantial Coulomb losses.

The cluster *nonthermal emission spectrum* can be obtained by combining the emission from individual DM halos. This requires a weighting with the halo velocity distribution function (as derived from N-body simulations) and with the mass function of galaxies in the cluster (see [9]). Because of the radial increase of the halo velocity dispersion and the radial decrease of the ICM gas density, the integrated nonthermal emission from supersonically moving halos will show an annular structure. The rings should be apparent well outside the central region where halos are expected to be slowed down by dynamical friction [41]. The picture is likely for clusters without any recent merging activity (as e.g. A2199)

Fig. 1 shows a simulated inverse-Compton and bremsstrahlung νF_ν spectra [9]. As the used model parameters can be considered typical for the Coma cluster, the result is consistent with the *BeppoSAX* flux measurements for Coma $\sim 1.4 \times 10^{-11}$ erg cm^{-2} s^{-1} (20-80 keV) deduced from [19]. Inverse-Compton radiation, bremsstrahlung, and synchrotron radiation by these electrons produce spectra that are in quantitative agreement with that observed from the Coma cluster. Moreover, the relative increase of hard X-ray emission outside the central 0.3–0.4 Mpc of the cluster A2199 can be understood in this framework.

In Fig. 2 the radio synchrotron spectrum of a cluster after averaging over the Mach-number probability distribution is shown [9]. The modelled radio synchrotron emission depends upon the inter-cluster magnetic field which was $\sim 0.1\mu$G [9]. The value is typical for all the models where the hard X-ray emission is due to Compton up-scattering of the 3K cosmic microwave background (CMB) radiation by radio emitting electrons (e.g. [46,19])). That is often considered as a potential shortcoming of the inverse Compton emission model, because of the magnetic field values of $\gtrsim \mu$G range deduced from Faraday rotation measurements of background radio sources (e.g. [24], but see also [40] for a critical review). While the CMB photon field dominates in most parts of a cluster volume there are also extended DM halos (e.g. massive galaxies) filled with the interstellar radiation field having substantial IR and optical components. That allows to model

the inverse Compton origin of hard X-ray emission from relatively low energy electrons (below the GeV regime), while the observed radio emission is produced by electrons above a few GeV in a μG magnetic field.

Recently we constructed a variant of the model [9] where mildly relativistic electrons (of Lorentz factors $\gtrsim$ 10) comprising the long-lived CR electron population in the ICM (c.f.[15]) are re-accelerated by the MHD-shocks from fast moving DM halos (or from a merging event). The model accounted for the diffusive shock acceleration and the second order Fermi acceleration in the post-shock flow. The energy efficiency problem is alleviated in the model in comparison with the case of direct particle injection from the thermal plasma. The modelled radio synchrotron emission spectrum reproduces that given in Fig. 2 for inter-cluster magnetic field $\sim 1\mu$G. The inverse Compton components were calculated under the assumption that the radiation fields of the fast moving halos are similar to that evaluated by [52] for the outer Milky Way (i.e. the CMB with substantial IR and optical photon fields). In Fig. 3 we show the IC components by the solid and dotted curves calculated under somewhat different ratios of the IR and optical fields. An alternative approach to reconcile the μG inter-cluster magnetic fields with diffuse hard X-ray and radio emission is to exploit unsteady nonthermal particle distributions (e.g. [44]).

A recently proposed project of a hard X/γ-ray (100 keV- 2 MeV) telescope – the Compton Cube [29] – could be used to test the predicted hard X-ray emission from clusters like Coma. With a modest angular resolution about 2 degrees, it could detect energy flux $\sim 10^{-11}$ erg cm^{-2} s^{-1} above 100 keV. Spatially resolved γ-ray spectra of clusters observed with the forthcoming *GLAST* mission could strongly constrain the energetic lepton component in the clusters.

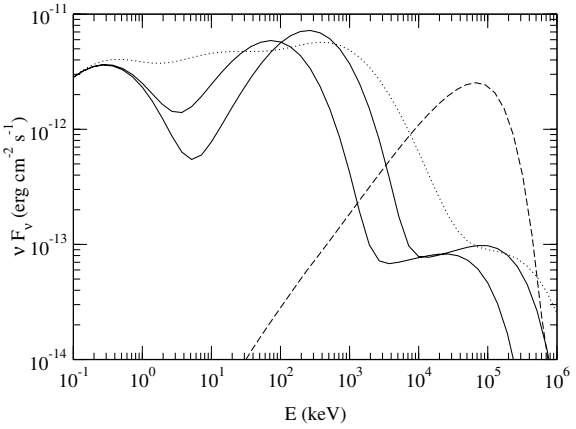

Figure 3. Nonthermal inverse Compton (the solid and dotted curves) and bremsstrahlung (dashed curve) spectra of an ensemble of fast moving halos with account of the re-acceleration of electrons from the ICM non-thermal pool.

3. NONTHERMAL EMISSION DUE TO MINIHALOS ACCRETION ON A MASSIVE GALAXY

The existence of DM satellites interacting with massive galaxies is a prediction of the CDM hierarchical model of cosmic structure formation (e.g. [42]). High resolution N-body simulations of DM substructure of the galactic halos (e.g. [28,36]) have predicted copious substructure DM satellites within galactic halos. Observational data concerning Local Group dwarf galaxies interactions (e.g. that reviewed in [33]) indicated that the predicted abundance of satellites of a circular velocity $v_c \lesssim 30$ km s^{-1} is higher than that of the observed dwarf galaxies population in the Local Group. A satellite with a bound mass M_b within a bound radius r_b has the circular velocity $v_c = (GM_b/r_b)^{1/2}$.

There are some ways to solve that problem in the frame of the CDM model. The suggested suppression of gas accretion and star formation in low-mass halos could be a solution of the dwarf satellite problem (e.g. [42] and the references therein). An elegant hypothesis concerning a possible link between the observed High Velocity Clouds (HVCs) and DM clumps was suggested in [4]. In that model HVCs originally detected due to their 21 cm radio emission are the "missing" DM halos and they are remnants of the Local

Group building blocks [4]. Another possible way to reconcile the hierarchical model predictions with dwarf galaxies observations is to suppress the small-scale end of the spectrum of primeval fluctuations of DM distribution.

It has been pointed out in [36] that the DM satellites are on orbits that take a large fraction of them through the stellar disk leading to a significant number of disk-satellite interactions. Thus it seems important to investigate possibilities of the presence of multiple low mass satellites orbiting within a virial radius of a galaxy. Those interactions result in accretion of low-metallicity gas, hitting the galactic disk and possibly generating nonthermal particle acceleration. The energy release of the infalling DM matter is $\gtrsim 10^{41}$ erg s^{-1} assuming the infalling velocity is $\gtrsim$ 200 km s^{-1}. Observations and some indirect arguments (e.g. [4]) point to present-day baryonic matter accretion rates of $\sim 1 M_\odot$ yr^{-1} and an associated DM accretion rate of $\sim 8 M_\odot$ yr^{-1}.

Fig. 4 shows the simulated νF_ν spectra of the galactic nonthermal diffuse emission due to large-scale shocks produced by accreting mini-halos (i.e. HVCs). We used the interstellar radiation field described in [52] to calculate the inverse-Compton emission of shock accelerated electrons. The bremsstrahlung contribution comes from the electron interaction with a galactic HI disk of half-thickness $\sim$ 100 pc. There are also other sources of the diffuse hard emission due to cosmic ray interactions with galactic matter and radiation (see e.g. [52] and references therein). However, nonthermal emission calculated for the local galactic cosmic ray spectra can not explain the *GRO EGRET* observation in the GeV regime (e.g. [52]). The contribution from the accreting DM satellites could be important to understand the apparent excessive emission in the GeV regime observed by *GRO EGRET*. On the other hand, the observations of diffuse high energy emission from the Milky Way and other massive galaxies could be a powerful tool to constrain the satellite-galaxy interactions. There is some observational evidence for an additional heat source in the warm ionized medium in the Galaxy [48]. The required heating rate is $\sim 10^{-25}$ erg cm^{-3} s^{-1} and should scale with the density of the ambient

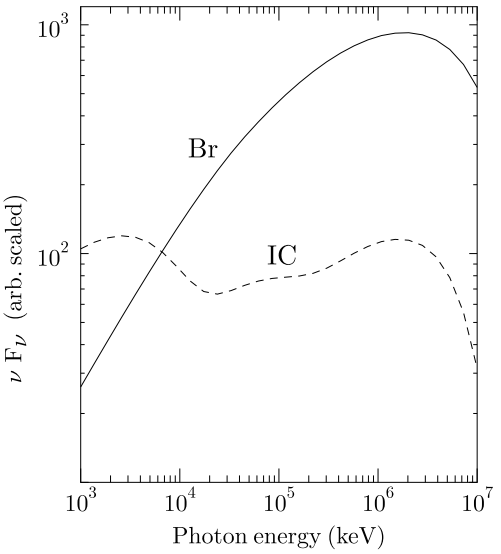

Figure 4. Simulated diffuse γ-ray emission from nonthermal electrons accelerated by large scale shocks produced by DM satellites accreting onto the Milky Way. The solid line is the bremsstrahlung emission and the dashed line is the inverse Compton.

electrons $\propto n_e^c$ with $c \leq 1$ [48], to supplement the gas heating due to photoionization which scales as $\propto n_e^2$. The heating due to accretion flow dissipation could help to solve the problem.

4. SNRs IN THE GALACTIC CENTER REGION

Supernova explosions in a dense ambient medium should result in fast conversion of the SN energy into emission (e.g., [59,12,10,8]). Interaction of a SNR with a molecular cloud manifests itself as a number of spectacular appearances in a wide range of wavelengths from radio to gamma-rays. The propagation of a radiative shock wave through a molecular cloud leads to a substantial non-thermal emission both in hard X-rays and in γ-rays. The complex structure of a molecular cloud consisting of dense massive clumps embedded in the interclump medium could result

in localized sources of hard X-ray/γ-ray emission correlated with bright molecular emission [8]. It has been shown that hard X-ray and γ-ray emission structure should consist of an extended shell-like structure (appearing also in radio as a shell with a relatively flat spectrum) related to the radiative shock and localized sources corresponding to shocked molecular clumps. The shocked clumps would have (sub)parsec scales and emit very hard X-ray continuum spectra. Here we shall discuss another phenomena of SN activity in the dense environment of the Galactic Center (GC) – a potentially abundant class of hard faint X-ray sources powered by interaction of fast moving knots with dense medium [7].

Recently the Galactic center region was deeply studied with the *Chandra* observatory [2,32,58,37, 38]. With a deep 590 ks *Chandra* exposure of a $17' \times 17'$ field in the GC region Muno et al. [37] catalogued 2357 X-ray sources limited in luminosity by $L_{\rm x} \geq 10^{31}$ erg s^{-1} (2.0–8.0 keV). A substantial part of the *Chandra* sample sources positions is projected into the Circum-Nuclear Disc [34] between 1.7 and 7 pc around the GC that contains $\sim 10^4 {\rm M}_\odot$ of highly clumped matter.

4.1. SN ejecta fragments

Multi-wavelength studies of SNRs have revealed a complex structure of metal ejecta with the presence of fast moving isolated fragments of SN ejecta, interacting with the surrounding media. In the optical the multiple fast moving knots (FMKs) were observed outside the main shell of Cas A (e.g.[11,16]) and in some other SNRs. Optical FMKs in Cas A are very abundant in O-burning and Si-group elements. They have a broad velocity distribution around 6,000 km s^{-1} and apparent sizes below 0.01 pc. The optical knots in Cas A should have $L_{\rm x} \leq 10^{29}$ erg s^{-1} because of the low ambient density. The similar FMKs in the dense environment of the GC region would have $L_{\rm x} \geq 10^{30}$ erg s^{-1} with bright IR counterparts [6]. In a low density medium only relatively big FMKs can be observed in X-rays, like the Vela shrapnel A. *Chandra* and *XMM-Newton* observations revealed there a head-tail structure with a prominent Si line, indicating that the object is a fast ejecta fragment of the scale $\sim$ 0.3 pc [1]. Some of the hard X-ray sources detected with *XMM-Newton* in IC 443 are likely to be fragments of the SN ejecta of size below 0.1 pc interacting with a molecular cloud border [5].

An ensemble of hard X-ray point-like sources associated with fast moving supernova ejecta fragments is abundant and can account for the observed properties of the detected GC sources such as the hardness ratios and the logN–logS distribution. We simulate X-ray spectra of the FMKs of different velocities in the GC environment. In our model the hard X-ray emission of FMKs is due to both hot thermal postshock plasma and nonthermal particles accelerated at the bow shock. The particles propagate through a metal-rich clump, producing K-shell ionization line photons and hard nonthermal bremsstrahlung. It should be noted that most of our simulations are relevant to any kind of FMKs that are not necessarily originating from SN activity. They could be ejected by compact objects like Sgr A* or other objects.

4.2. X-ray emission of FMKs in the Galactic Center region

Consider an FMK propagating through the intercloud gas which pervades the central 50 pc with an estimated average density of some 10^2 cm^{-3} and an atomic hydrogen mass of $\sim 10^6 {\rm M}_\odot$ [34]. That is about one half of the total mass in this region. The matter is highly clumped. The magnetic field in the GC region is of mG strength, and provides a substantial contribution to the total pressure.

There are many early-type stars in the GC with more than two dozens of blue supergiants, providing the luminosity of the central parsec of $\sim 10^8 \, {\rm L}_\odot$, supernova remnants, dense molecular clouds, extended magnetic structures, evidence for high star-forming activity in the past (a few 10^7 years ago) (e.g., [34]).

Massive star winds would change the circumstellar environment, creating caverns of low density matter. In that case the lifetime of fast fragments of a core-collapsed SN should be longer than $R_{\rm b}/v_{\rm k}$, where $R_{\rm b}$ is a wind bubble size. The typical scale is $R_{\rm b} \sim 3$ pc for a WR star, while $R_{\rm b}$ is ~ 1 pc for O9-B0 progenitor stars in the GC environment. The corresponding lifetimes

are $\sim 10^3$ years. The collective effect of powerful stellar winds in compact associations could blow out more extended caverns, providing somewhat longer lifetime of the fragments of the SNe exploded inside the cavern.

The lifetime of an FMK in a dense medium is an important factor for the model. A fast moving knot is decelerating due to the interaction with the ambient gas. The drag deceleration time of a knot of velocity v, mass $\mathcal{M}$ and radius $\mathcal{R}$ can be estimated as $\tau_{\rm d} \approx 10^3 \cdot \mathcal{M}_{-3}/(n_{\rm a2}\, v_8\, \mathcal{R}^2_{-2})$ years. Here $\mathcal{M}_{-3} = \mathcal{M}/10^{-3}\,{\rm M}_\odot$ and $\mathcal{R}_{-2} = \mathcal{R}/(0.01$ pc). The number density $n_{\rm a2}$ of the ambient matter is measured in 100 cm^{-3} and the FMK velocity v_8 is measured in 1,000 km s^{-1}. In the inner $20'$ of the GC region the average number density $n_{\rm a} \gtrsim 100$ cm^{-3} (e.g. [34]) and the fragment deceleration time $\tau_{\rm d} \lesssim 10^3$ years.

The high pressure gas in the head of a fast moving ejecta fragment could drive an internal shock resulting in the knot crush and fragmentation (e.g.[27,57]). The fragmentation time scale could be somewhat less than the drag deceleration time $\tau_{\rm d}$. However, the FMK will be a source of hard X-ray emission even at the fragmented stage if the strong forward shock is still driven by the FMK. The effects of nonthermal particle acceleration reduce the postshock gas pressure and the internal shock velocity, thus increasing the crushing time [6]. In that case the life time would be close to $\tau_{\rm d}$, unless the ablation processes. The effect of magnetic fields and nonthermal particles on the knot ablation is not yet studied.

Supersonic motions of the FMKs in the ambient medium result in a bow-shock/knot-shock structure heating the postshock plasma and accelerating the fast particles. Both thermal and nonthermal emission of postshock plasma can produce X-ray photons.

4.3. Thermal emission of FMKs

Thermal emission of the hot postshock plasma could be observed from some FMKs even from the highly obscured GC region. The postshock ion temperature (measured in 10^7 K) can be estimated as $T_{\rm i7} \approx 1.4\, v_8^2$ for the simplest single-fluid case of a plasma of the solar abundance. The electron temperature just behind a strong shock is typically much lower. In the postshock layer the electron and ion temperatures equilibrate due to Coulomb collisions on a timescale $t_{\rm ei}$. The maximum electron temperature in the postshock region can be estimated from the relation $\tau_{\rm d} \geq t_{\rm ei}$ providing $T_{\rm e7}^{\rm max} \leq 7 \cdot \mathcal{M}_{-3}^{1/2} \cdot \mathcal{R}_{-2}^{-1}$. Note that the maximal electron temperature can be achieved only for FMKs with $v_8 \geq 2.3 \cdot \mathcal{M}_{-3}^{1/4} \cdot \mathcal{R}_{-2}^{-1/2}$.

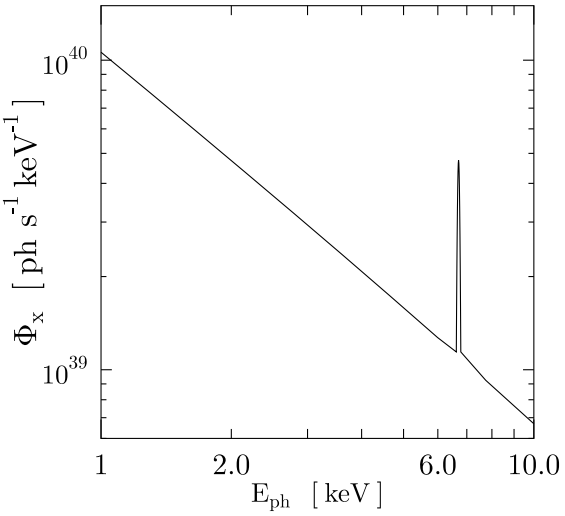

Figure 5. Simulated spectrum of nonthermal emission of an FMK of mass $\mathcal{M} \approx 10^{-3}{\rm M}_\odot$, (with $\sim 10^{-4}{\rm M}_\odot$ of Fe) in an ambient medium of n = 100 cm^{-3}. Radius is $\mathcal{R} = 3 \times 10^{16}$ cm and velocity $v \approx 5,000$ km s^{-1} [7].

Thermal bremsstrahlung luminosity of the thin postshock plasma $L_{\rm Tx}$ is $\sim 6 \cdot 10^{31} \cdot \mathcal{R}^3_{-2} \cdot n^2_{\rm a2} \cdot T^{1/2}_{\rm e8}$ erg s^{-1}.The FMKs of that luminosity can be observed from the GC region with *Chandra* and *XMM-Newton* . Note that $L_{\rm Tx} \propto n_a^2$ and thus we have much better chances to observe the X-ray emission from individual FMKs in the GC region. In the low density medium only a collective emission of multiple FMKs could be detected.

4.4. Nonthermal emission of FMKs

Energetic nonthermal particles accelerated by the Fermi mechanism in MHD collisionless shocks diffuse through the hot postshock layer and a cold

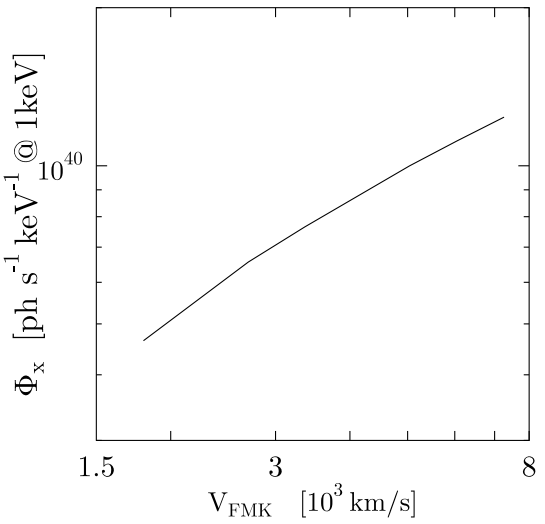

Figure 6. The nonthermal X-ray continuum luminosity (at 1 keV) of FMKs of different velocities v in an ambient medium of n = 100 cm^{-3}.

body of a metallic knot, suffering from Coulomb losses and producing hard X-ray emission both in lines and continuum [6]. The accelerated electron distribution was simulated using the kinetic description of charged particles interacting with a strong MHD shock. The X-ray line emission is due to K-shell ionization by nonthermal and thermal particles accelerated by the bow shock and then propagating through a metal-rich clump. Mildly relativistic particles have a high penetrating ability in the knot and the K-shell ionization cross-section has an upturn near relativistic electron energies [6]. Compact dense knots could be opaque for some X-ray lines. The optical depth effect due to resonant line scattering is important and is accounted for in the model [6].

In Fig. 5 we present a simulated spectrum of the nonthermal X-ray emission from an FMK of size 0.01 pc size and mass $\mathcal{M} \approx 10^{-3}$ M$_\odot$ dominated by oxygen and containing about $\sim 10^{-4}$ M$_\odot$ of Fe. The knot of velocity $v = 5,000$ km s^{-1} is moving through an ambient gas of $n_{\rm a} = 10^2$ cm^{-3}.

The nonthermal bremsstrahlung spectrum in Fig. 5 is a power law of photon index $\Gamma \approx 1.2$ with a prominent Fe line. The photon index depends on the model of particle diffusion inside the FMK and the rate of nonthermal ions injection [6], with indices between 0 and 1.5 [7].

In Fig. 6 we show the simulated dependence of the nonthermal X-ray luminosity on the fragment velocity for the same FMK model. The power-law scaling $L_X \propto v^\zeta$ with $\zeta \approx 0.6$ fits the simulated data for the FMK velocity range $1.8 < v_8 < 7$.

Any SN event in the GC region is expected to produce many hundreds of fast moving fragments of mass $\sim 10^{-3}$M$_\odot$. If a SN ejects $\mathcal{N}_\star \sim$ 500 FMKs of velocity 5,000 km s^{-1}, the FMKs would carry about 10% of the SN kinetic energy. Three SNRs during the last 1000 years could produce an ensemble of more than 1,500 FMKs in the GC region providing a normalization of the logN–logS distribution. The logN–logS distribution index and the hardness ratios of the FMKs [7] are consistent with the *Chandra* findings.

Fast moving SN ejecta fragments interacting with the dense GC environment provide a fast conversion of SN kinetic energy into IR and X-ray emission. The X-ray spectra of the fragments (with L$_{\rm x} \leq 10^{33}$ erg s^{-1} per FMK) are hard. They contain thermal and power law components with possible Fe lines. Both 6.7 and 6.4 keV lines are expected, depending on the FMK ionization structure and the relative strength of the nonthermal component. The total equivalent width is about 500 - 600 eV for a Fe mass of $\sim 10^{-4}$ M$_\odot$. The hardness ratios $hr = (h - s)/(h + s)$ were simulated. The numbers of counts in the high energy band h (4.7–8.0 keV) and low band s (3.3–4.7 keV) were chosen for hard color, and h (3.3–4.7 keV) and s (2.0–3.3 keV) for medium color.

The spatial density of the FMKs brighter than some fixed luminosity $\mathcal{L}_0$ scales as $\propto n_{\rm a}^\gamma(r)$ with the ambient gas density. This is because $L_{\rm x} \propto n_{\rm a}^\nu$ for a single FMK,while the lifetime $\propto n_{\rm a}^{-1}$. The index $\gamma = -\nu(\alpha + 1) - 1$ depends on the logN–logS distribution index α. For the thermal emission model $\nu = 2$. This implies a global decrease in the spatial density of the sources $\propto n_{\rm a}^{0.4}(r)$ (for $\alpha = -1.7$) away from Srg A*, though strong local fluctuations could appear. The apparent surface density of the FMKs would depend on the symmetry of the SN distribution (e.g. disk or

spherical). The global distribution of the FMKs in the GC is expected to be an ensemble of coherent shell- and jet-like structures of scale a few arcminutes.

The ensemble of unresolved faint knots of galactic supernovae can contribute substantially to the hard continuum and the iron line emission observed from the Galactic Center region and the Galactic ridge (c.f. [54]).

I am very grateful to the Symposium organizers for a very interesting meeting and kind support. The work was supported by RBRF 03-02-17433, 01-02-16654 and INTAS-ESA 99-1627 grants.

REFERENCES

1. B. Aschenbach In: Neutron Stars, Pulsars and Supernova Remnants. eds. W.Becker et al. , MPE, p.13, 2002.
2. F.K.Baganoff, et al. ApJ 591 (2003) 891.
3. V.S. Berezinsky, P.Blasi, V.S.Ptuskin, ApJ 487 (1997) 529.
4. L.Blitz et al. , ApJ 514 (1999) 818.
5. F.Bocchino, A.M.Bykov, A&A 400 (2003) 203.
6. A.M.Bykov, A&A 390 (2002) 327
7. A.M.Bykov, A&A 410 (2003) L5
8. A.M. Bykov, R.A. Chevalier, D.C.Ellison, Yu.A. Uvarov, ApJ 538 (2000) 203.
9. A.M. Bykov, H.Bloemen, Yu.A.Uvarov, A&A 362 (2000) 886.
10. R.A.Chevalier, ApJ 511 (1999) 798
11. R.A.Chevalier, R.P.Kirshner, ApJ 233 (1979) 154
12. B.T.Draine, D.T.Woods ApJ 383 (1991) 621
13. S.Colafrancesco, P.Blasi, Astropart. Phys. 9 (1998) 227.
14. F.Durret et al. , A&A 390 (2002) 397.
15. T.A. Enßlin, R.A. Sunyaev, A&A 383 (2002) 423.
16. R.Fesen et al. , AJ 122 (2002) 2644.
17. A.Finoguenov et al. , A&A 410 (2003) 777.
18. M.Fujita, M.Takizawa, C.L.Sarazin, ApJ 584 (2003) 190.
19. R.Fusco-Femiano et al. , ApJ 513 (1999) L21.
20. R.Fusco-Femiano et al. , ApJ 534 (2000) L7.
21. R.Fusco-Femiano et al. , ApJ 552 (2001) L97.
22. R.Fusco-Femiano et al. , astro-ph/0207241.
23. G.Giovannini et al. , ApJ 406, (1993) 399.
24. G.Giovannini, L.Feretti, New Astronomy, 5 (2000) 335.
25. J.S.Kaastra et al. , ApJ, 519 (1999) L119.
26. J.S.Kaastra et al. , A&A, 365 (2001) L99.
27. R.I. Klein, C.F.McKee, P.Colella, ApJ 420 (1994) 213.
28. A.Klypin, et al. ApJ 522 (1999) 82.
29. F.Lebrun et al. , Nucl. Instr. Meth. A 504 (2003) 38.
30. H.Liang, V.A.Dogiel, M.Birkinshaw, MNRAS 337 (2002) 567.
31. R.Lieu, et al. , ApJ 458 (1996) L5.
32. Y.Maeda et al. , ApJ 570 (2002) 671.
33. M.L.Mateo, ARA&A 36 (1998) 435.
34. P.G.Mezger et al. , AARev 7 (1996) 289.
35. F.Miniati et al. ApJ 542 (2000) 608.
36. B.Moore, et al. ApJ 524 (1999) L19.
37. M.P.Muno et al. , ApJ 589 (2003) 225.
38. M.P.Muno et al. , astro-ph/0308335, (2003).
39. D.M.Neumann et al. , A&A, 365 (2001) L74.
40. W.I.Newman et al. , ApJ, 575 (2002) 755.
41. T.Okamoto, A.Habe, ApJ 516 (1999) 591.
42. J.P.Ostriker, P.Steinhardt, Science 300 (2003) 1909.
43. J.R.Peterson et al. , A&A 365 (2001) L104.
44. V.Petrosian ApJ 557 (2001) 560.
45. O.Reimer et al. , ApJ 588 (2003) 155.
46. Y. Rephaeli, ApJ, 227 (1979) 364.
47. Y.Rephaeli, et al. ApJ, 429 (1994) 554.
48. R.J.Reynolds et al. , ApJ 525 (1999) L21.
49. K. Roettiger, et al. ApJ 518 (1999) 603.
50. C.L.Sarazin, ApJ 520 (1999) 529.
51. P.Sreekumar et al. , ApJ 464 (1996) 628.
52. A.W.Strong, I.V.Moskalenko, O.Reimer, ApJ 537 (2000) 763.
53. T.Tamura et al. , A&A 365 (2001) L87.
54. Y.Tanaka, T.Miyaji, G.Hasinger, Astron. Nachr. 320 (1999) 181
55. A.Vikhlinin, et al. ApJ 551 (2001) 160.
56. H.J.Völk, A.M.Atoyan, ApJ 541 (2000) 88.
57. C.Wang, R.A. Chevalier ApJ 574 (2002) 155
58. Q.D.Wang, E.V, et al. Nature 415 (2002) 148.
59. J.C.Wheeler et al. , ApJ 237 (1980) 781.
60. D.A.White, C.Jones, W.Forman, MNRAS, 292 (1997) 419.
61. S.D.M.White, M.Rees, MNRAS, 183 (1978) 341.